AD-A087 941 IOWA UNIV IOWA CITY DEPT OF PHYSICS AND ASTRONOMY F/G 3/2
THE ENERGETIC CHARGED PARTICLE ABSORPTION SIGNATURE OF MIMAS.(U)
JUL 80 J A VAN ALLEN, M F THOMSEN N00014-76-C-0016
UNCLASSIFIED U. OF IOWA-80-15 NL

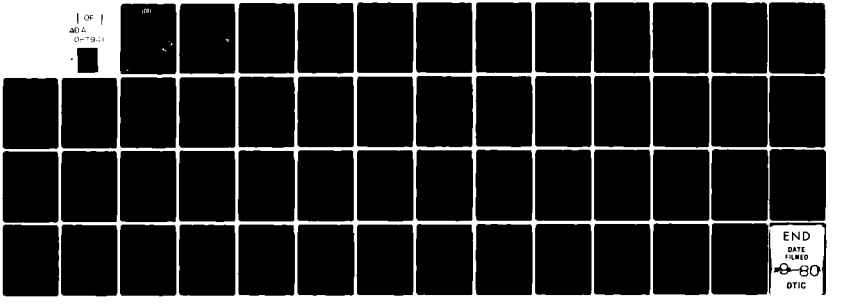

END
DATE FILMED
9-80
DTIC

LEVEL II

12

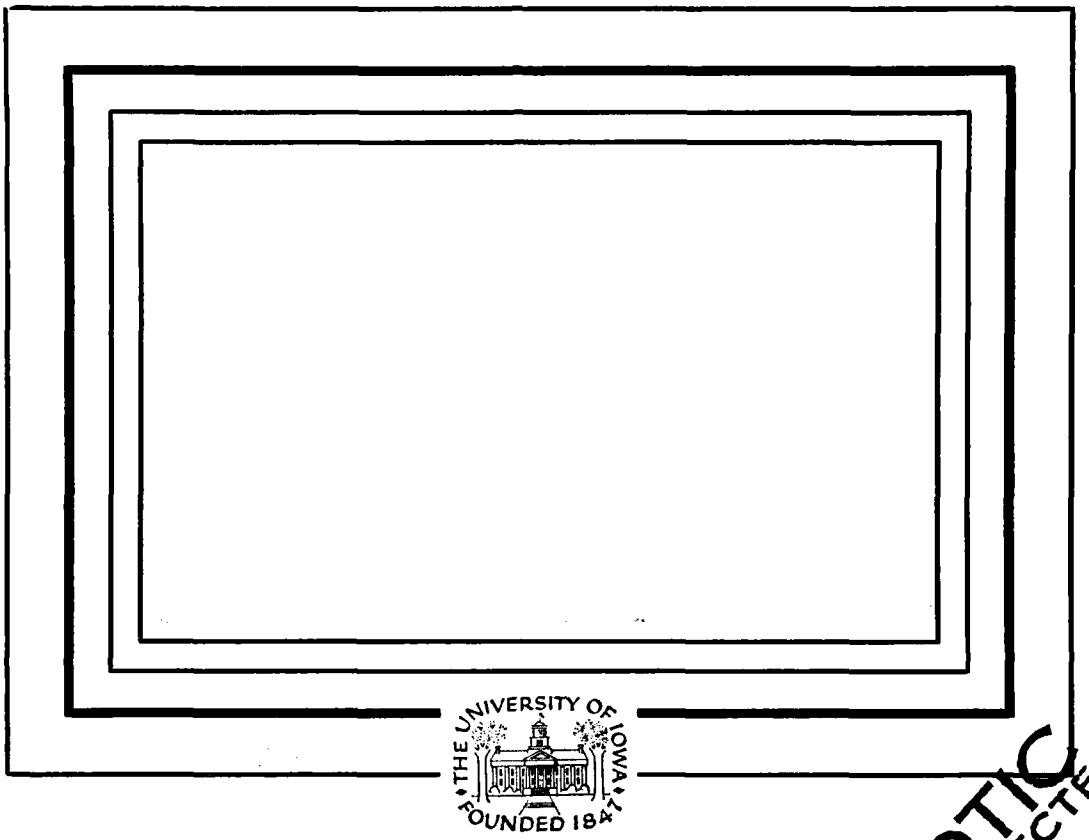

Department of Physics and Astronomy

THE UNIVERSITY OF IOWA

Iowa City, Iowa 52242

12

U. of Iowa 80-15

The Energetic Charged Particle Absorption Signature of Mimas

by

J. A. VAN ALLEN, M. F. THOMSEN,
and B. A. RANDALL

Department of Physics and Astronomy
The University of Iowa
Iowa City, Iowa 52242

19 July 1980

Second revision of original manuscript of 30 April 1980.

In press, J. Geophys. Res., 85, 1980.

UNCLASSIFIED

SECURITY CLASSIFICATION OF THIS PAGE (When Data Entered)

REPORT DOCUMENTATION PAGE	READ INSTRUCTIONS BEFORE COMPLETING FORM
1. REPORT NUMBER: U. of Iowa 80-15 / 2. GOVT ACCESSION NO.: AD-A087941	3. RECIPIENT'S CATALOG NUMBER:
4. TITLE (and Subtitle): The Energetic Charged Particle Absorption Signature of Mimas.	5. TYPE OF REPORT & PERIOD COVERED: Progress, July 1980
	6. PERFORMING ORG. REPORT NUMBER: --
7. AUTHOR(s): J. A. Van Allen, M. F. Thomsen and B. A. Randall	8. CONTRACT OR GRANT NUMBER(s): N00014-76-C-0016
9. PERFORMING ORGANIZATION NAME AND ADDRESS: Department of Physics and Astronomy, The University of Iowa, Iowa City, Iowa 52242	10. PROGRAM ELEMENT, PROJECT, TASK AREA & WORK UNIT NUMBERS: --
11. CONTROLLING OFFICE NAME AND ADDRESS: Office of Naval Research, Electronics Program Office, Arlington, Virginia 22217	12. REPORT DATE: 19 July 1980 / 13. NUMBER OF PAGES: 51
14. MONITORING AGENCY NAME & ADDRESS (if different from Controlling Office)	15. SECURITY CLASS. (of this report): UNCLASSIFIED / 15a. DECLASSIFICATION/DOWNGRADING SCHEDULE

16. DISTRIBUTION STATEMENT (of this Report)

Approved for public release; distribution unlimited.

17. DISTRIBUTION STATEMENT (of the abstract entered in Block 20, if different from Report)

18. SUPPLEMENTARY NOTES

To be published in J. Geophys. Res.

19. KEY WORDS (Continue on reverse side if necessary and identify by block number)

Magnetosphere of Saturn
Saturn
Mimas

20. ABSTRACT (Continue on reverse side if necessary and identify by block number)

[See page following.]

DD FORM 1 JAN 73 1473 EDITION OF 1 NOV 65 IS OBSOLETE
S/N 0102-LF-014-6601

UNCLASSIFIED
SECURITY CLASSIFICATION OF THIS PAGE (When Data Entered)

ABSTRACT

Data are presented for a one-minute dip in electron intensity that was observed coherently by four different ~~University of Iowa~~ detectors at 1546:51 ERT on DOY 244/1979 as Pioneer 11 crossed the orbit of Mimas inbound during its encounter with the Saturn system. By a detailed analysis, we show that ~~(a)~~ this absorption microsignature in electron intensity is plausibly attributable to the particle sweeping effect of Mimas; ~~(b)~~ the radial width of the signature is caused primarily by energy dispersion in the longitudinal drift rate of electrons and not by radial diffusion; ~~(c)~~ the spectrum of trapped electrons at Mimas is nearly monoenergetic, centered at kinetic energy E = 1.59 MeV with a spread $\delta E \sim 0.1$ MeV; ~~(d)~~ this narrow spectrum, which is unique in magnetospheric physics, is caused by the "band-pass filtering" action of the successive inner satellites, most importantly Enceladus, on an inward diffusing population of electrons; and ~~(e)~~ the radial diffusion coefficient D of electrons E = 1.0 MeV is 1.0×10^{-10} R_s^2/s^{-1} at L = 4 and probably in the range 3.7 ~~$\times 10^{-11}$~~ to 8.3×10^{-12} R_s^2/s^{-1} at L = 3.

Accession For	
NTIS GRA&I	☑
DDC TAB	☐
Unannounced	☐
Justification	
By	
Distribution/	
Availability Codes	
Dist	Avail and/or special
A	

Introduction

A satellite orbiting within a planet's magnetosphere causes a number of interesting and complex phenomena which provide unique information on particle diffusion and other dynamical processes. Pioneer and Voyager observations have shown that Jupiter's satellite Io is a spectacular example and that others of Jupiter's satellites also interact with the magnetosphere. The August/September 1979 flyby of Saturn by Pioneer 11 revealed the existence of a Saturnian magnetosphere and provided many examples of the absorption of trapped particles by its inner satellites, some of which were previously unknown [Fillius et al., 1980; Simpson et al., 1980a; Trainor et al., 1980; Van Allen et al., 1980a, b].

Mead [1972] discussed such absorption processes in Jupiter's magnetosphere prior to the first in situ observations by Pioneer 10. Subsequent authors gave further calculations of effects on the intensities of charged particles trapped in the Jovian radiation belt [Jacques and Davis, 1972; Mead and Hess, 1973; Hess et al., 1973, 1974]. Observations by Pioneers 10 and 11 confirmed the importance of satellite absorption effects and provided much detail [Thomsen, 1979].

Since the Pioneer flybys of Jupiter, a number of authors have used the observed satellite signatures in the energetic particle data to deduce diffusion coefficients for the radial transport of

trapped radiation [Simpson et al., 1974; Mogro-Campero and Fillius, 1974, 1976; Thomsen and Goertz, 1975; Thomsen, 1976; Mogro-Campero, 1976; Thomsen, 1977; Thomsen et al., 1977a, b]. These analyses were concerned with what may be called the "macrosignature" of the satellite, i.e., the average effect that the satellite has on the distribution of trapped radiation over a fairly long time scale (quasi-stationary state).

Van Allen et al. [1980b] have deduced that the counting rates of the University of Iowa detectors C and D in the inner magnetosphere of Saturn are primarily attributable to protons with energy greater than about 80 MeV. Such energetic protons have very large gyroradii (~ 2000 km) at the magnetic field strengths found in Saturn's inner magnetosphere ($L \sim 3$). Because of complexities introduced into the satellite sweep-up geometry by such large gyroradii, we defer to a later paper a full analysis of the macrosignatures of satellite sweeping at Saturn. In the present paper we first make a few remarks on the macrosignature of Mimas and then focus attention on a "microsignature" of satellite absorption, specifically a brief dip in the charged particle intensities observed on the inbound pass of Pioneer 11 as it passed through the orbital range of the satellite Mimas. This feature, which lasted only about 1 minute, was first noted by Simpson et al. [1980a], who remarked that it could not be a direct "shadow" of Mimas because Mimas was a considerable fraction of its orbit away from Pioneer 11 at that time.

In this paper we develop the hypothesis that this microsignature is indeed the "shadow" of Mimas, not in the sense that the spacecraft passed through the magnetic flux tube containing the satellite, but rather in the sense that the observations reveal the effect of the satellite on a distribution of particles which interacted with it at some time in the recent past and then drifted in longitude (by means of corotation, gradient, and curvature drifts) to the observational location. Such a point of view leads us to a characterization of the electron energy spectrum in Saturn's inner magnetosphere and to an estimate of the radial diffusion coefficient for such electrons.

Macrosignature

Figure 1 shows frame-by-frame counting rates for detectors A, B, C, and D of the University of Iowa's Geiger Tube Telescope (UI/GTT) on Pioneer 11 for the time intervals during which the spacecraft was traversing the orbital location of Saturn's satellite Mimas. (See Van Allen et al. [1980b] for a description of the instrumentation.) Detectors A and B are directional detectors, and the large-amplitude oscillations in the A and B counting rates are caused by a very anisotropic pitch angle distribution. The period of the oscillations is the beat between the spacecraft rotation period and the detector sampling period. Maximum intensities are observed when the detectors are sampling pitch angles near 90° and minimum intensities are observed near 0° and 180° (pancake distribution).

Detectors C and D are omnidirectional detectors and hence show little periodic modulation. Also shown in Figure 1 are the 115.5 second (14 sample) averages of the counting rates. A sequence of fourteen samples provides approximately complete pitch angle coverage; so these averages eliminate the modulation due to the anisotropy of the distribution.

The broad depressions in intensity observed by detectors C and D within the radial range of Mimas' slightly eccentric orbit constitute what we call the macrosignature of charged particle absorption by Mimas. There is potentially a great deal of information in these macrosignatures, but as indicated earlier, we defer a detailed discussion of them to a later paper. One striking feature seen in Figure 1 is the qualitatively different nature of the curves for detectors C and D and those for detectors A and B. Outbound, detectors A and B show no depression in their average counting rates at Mimas' orbit. On the inbound crossing, these detectors both show only a slight indication of a broad macrosignature but exhibit a dramatic dip in counting rate within a brief time interval around 1547 ERT. Detectors C and D also exhibit clear counting rate dips at 1547 ERT, though not with as good statistical accuracy as do detectors A and B. This brief dip is the microsignature that we will be discussing. In contrast to the apparent absence of a macrosignature in detectors A and B, detectors C and D show broad and deep reductions in intensity, both inbound and outbound. Furthermore, the macrosignatures in detectors C and D have

relatively flat minima, covering essentially the entire radial range of Mimas in its eccentric orbit (horizontal bar in Figure 1).

As discussed by Van Allen et al. [1980b], we attribute this difference in macrosignatures to the fact that within the inner magnetosphere detectors C and D are responding primarily to protons with energies above 80 MeV, whereas A and B are counting primarily electrons with energies of the order of 1 MeV. Thus, we can understand the marked difference in the macrosignatures shown for the various detectors in Figure 1 in terms of differences in the gyroradii and longitudinal drift rates of the particles being observed. In particular, the gyroradius of an 80 MeV proton near the orbit of Mimas is ~ 2000 km (0.033 R_s), whereas that of a 1 MeV electron is only ~ 7 km. The effective sweeping radius of a nonconducting satellite is approximately the sum of its geometric radius (~ 180 km for Mimas [Cruikshank, 1978] and the particle's gyradius [see, e.g., Thomsen et al., 1977a]. Hence, the satellite absorbs high energy protons over a much greater spatial region than it does low energy electrons. Furthermore, the angular velocity in longitude (due to corotation, gradient and curvature drifts) of 80 MeV protons relative to Mimas is ~ 10^{-2} radian s^{-1}, whereas that of ~ 1 MeV electrons is several orders of magnitude less (almost "synchronous" with the satellite's orbital motion [Thomsen and Van Allen, 1980]). As a consequence, high energy protons encounter the satellite much more frequently and therefore suffer far greater losses.

On the basis of these arguments, we interpret the macrosignatures of Mimas in detectors C and D as a true stationary state resulting from essentially total absorption of high energy ($\geq$ 80 MeV) protons within the orbital range of Mimas. This interpretation is consistent with the findings of Fillius et al. [1980]. As discussed by Van Allen et al. [1980b], we further interpret the residual counting rates of C and D in the relatively flat minima of their Mimas macrosignatures as being due to electrons, for which satellite absorption is not nearly as effective as for high energy protons. This latter fact is evidenced by the generally slight absorption effect seen in detectors A and B. Van Allen et al. [1980b] note that in this region detectors C and D might be responding either to direct penetration by electrons with energies greater than 20 - 30 MeV or, much more likely, to bremsstrahlung arising from lower energy electrons ($\sim$ 1 - 2 MeV). In this paper we find strong support for the latter possibility.

Microsignature

One of the most striking features of Figure 1 is the coherent decrease in intensity observed by all detectors for about 1 minute at 1547 ERT on the inbound crossing. No such feature is observed (Figure 1) during the outbound crossing, in agreement with Simpson et al. [1980a].

The time dependence of the counting rate of the omnidirectional detector C, normalized to the trend line through the data on both sides of the dip, is shown in Figure 2. The nature of the fitted

curve is discussed later. Because of the strong modulation of the counting rates of the directional detectors A and B, the preparation of a composite curve for all three detectors is more difficult. (The data from D are concordant but are of such low statistical accuracy as to contribute little to the shape of the profile.) For this purpose we normalized the A and B rates to an angular distribution function that was determined from the raw pitch angle dependence of the counting rates just before and just after the microsignature. Figure 3 shows an example of data obtained by detector B just after the microsignature. The solid line shows an analytical expression that represents the observed points quite well. The shape of this function also fits well the data observed just prior to the microsignature, although the overall intensity was somewhat lower. The expression given in Figure 3 was adopted as the normalizing function for the microsignature points. The radial dependence of the resulting normalized set of data points was then removed by dividing by the least-squares fit of the spin-averaged data before and after the signature to a function linear in radial distance. A similar procedure was used for detector A, but the detector C data needed to be normalized only by the radial distance fit. The resulting set of normalized data points for detectors A, B, and C is shown in Figure 4. The statistical counting errors for C are the same as in Figure 2, but they are less by about a factor of 10 for A and B (Figure 1).

We interpret the signature shown in Figure 4 as a "hole" in the population of charged particles, which was created by the satellite during the most recent encounter of these particles with it. Such a hole is viewed as being created by satellite sweep-up in the manner envisioned by Mead [1972]; i.e., any particle whose trajectory (which is a combination of gyration about the field line, latitudinal bounce along the field line, and longitudinal drift) intersects the satellite is absorbed by it. Neighboring particles whose trajectories do not intersect the satellite continue their longitudinal drift, providing the undisturbed boundaries of the "shadow" of depletion. Successive holes drift in longitude at the drift rate of the missing particles to form an extended locus or "shadow". The shadow is: (a) gradually filled in by particles diffusing radially into it from the surrounding reservoir in response to fluctuating magnetic and/or electric fields and (b) progressively washed out by energy and pitch-angle dispersion in drift rate. As a function of increasing longitude downstream from the point of origin, the shadow becomes broader in radial width and shallower in depth, eventually disappearing altogether. The rates at which these two processes occur provide unique information on radial diffusion coefficients and on the identity and energy spectrum of the particles under study. We have not yet succeeded in solving the problem of simultaneous diffusion and dispersion but treat the two processes separately and then combine the results semi-intuitively.

Radial Diffusion

Diffusional fill-in can be modeled approximately by use of the one-dimensional diffusion equation:

$$\frac{\partial^2 y}{\partial x^2} = \frac{1}{D} \frac{\partial y}{\partial t} \qquad (1)$$

where $y(x,t)$ is the normalized charged particle number density, x is the radial distance, t is the time, and D is the diffusion coefficient for radial transport (here assumed independent of x over a small range of x and of particle energy E). The initial value of $y(x,t)$ at $t = 0$ must be specified by a model for the radial profile created during the encounter with the satellite. The simplest initial profile is a square well of width twice the radius b of the absorbing satellite (i.e., one for particles whose gyroradius $\rho \ll b$) and of depth unity.

The solution of equation (1) for this case is given both analytically and graphically in Figure 5 as a function of x and the dimensionless parameter

$$\tau \equiv \frac{4Dt}{b^2} . \qquad (2)$$

The minimum χ^2 fit of the function $y(x,t)$ shown in Figure 5 to the data of Figure 2 yields $\tau = 7.8 \pm 1.0$ and $b = 130 \pm 20$ km. As will be shown later, the appropriate value of t is 6.44 hr. Using these three numbers, we find an apparent value of the diffusion coefficient,

$D = 1.4 \times 10^{10}$ cm^2 s^{-1} or $D = 3.9 \times 10^{-10} R_s^2$ s^{-1}. In subsequent sections it will be seen that this value of D is in the nature of an upper limit because dispersion has not yet been introduced into the analysis. The effect of dispersion is to markedly reduce the requirement for diffusive effects and hence to reduce the inferred value of D by at least an order of magnitude.

For $\rho \geq b$, the gyrophase-averaged initial profile is of the form

$$y(x,t=0) = \begin{cases} 0 & \text{for} \quad |x| < b \\ \frac{1}{\pi} \arccos[1 - (|x| - b)/\rho] & \text{for} \quad b < |x| < (b + 2\rho) \\ 1 & \text{for} \quad (b + 2\rho) < |x| \end{cases} . \tag{3}$$

As before, x is the radial distance from the center of the swept-out region, b is the satellite radius, and ρ is the gyroradius of the charged particles. This function makes an analytical solution to Equation (1) quite intractable. However, it resembles and can be approximated by a simple trapezoidal shape, which is analytically manageable. The appropriate initial profile is thus approximately

$$y(x,t=0) = \begin{cases} 0 & \text{for} \quad |x| < b \\ (|x| - b)/2\rho & \text{for} \quad b < |x| < (b + 2\rho) \\ 1 & \text{for} \quad (b + 2\rho) < |x| \end{cases} . \tag{4}$$

With Equation (4) as the initial condition, Equation (1) can be solved analytically. The solution is

$$y(x,t) = 1 + \left(\frac{x - b - 2\rho}{4\rho}\right)\mathrm{erf}\left(\frac{b + 2\rho - x}{\sqrt{4Dt}}\right) - \left(\frac{x + b + 2\rho}{4\rho}\right)\mathrm{erf}\left(\frac{b + 2\rho + x}{\sqrt{4Dt}}\right) - \left(\frac{x - b}{4\rho}\right)\mathrm{erf}\left(\frac{b - x}{\sqrt{4Dt}}\right) + \left(\frac{x + b}{4\rho}\right)\mathrm{erf}\left(\frac{b + x}{\sqrt{4Dt}}\right) + \sqrt{\frac{Dt}{4\pi\rho^2}}\left[e^{-(b-x)^2/4Dt} + e^{-(b+x)^2/4Dt} - e^{-(b+2\rho-x)^2/4Dt} - e^{-(b+2\rho+x)^2/4Dt}\right] . \quad (5)$$

For several values of the particle gyroradius, ρ, the observed normalized data of Figure 4 have been compared to the analytical solution (5) for various sets of parameters (b,τ), where $\tau \equiv 4Dt/b^2$. The mean squared deviation of the observed points from the theoretical curve is found to be a minimum for a particular set (b,τ) for each value of the gyroradius. For example, for ρ = 10 km (corresponding to electrons with E $\approx$ 1.7 MeV), the best fit is obtained with (b = 90 km, τ = 12). This solution is shown as the solid line in Figure 4. For ρ = 50 km (E $\approx$ 10 MeV), the best fit is (b = 50 km, τ = 40). This solution is virtually identical to that shown in Figure 4 for ρ = 10 km. In general, the fits are not very sensitive to ρ for $\rho \leq$ 100 km but are significantly poorer at larger ρ. Furthermore, the best fits tend to give $(\rho + b) \approx$ 100 km.

Thus, even for $\rho = 0$ the estimated radius of Mimas is only about 100 km. This maximum radius is considerably smaller than the value of 180 km estimated from its optical albedo and mass [Cruikshank, 1978]. Thus, it appears that in this simple picture the observed profile is narrower than it ought to be, given the amount of refilling that has apparently occurred. It is clear from Figure 5 that, for a given b, the depth of the profile is the feature that is the most influential in determining τ. Again using Equation (2), we find that $D \sim 3 \times 10^{-10} R_s^2 s^{-1}$ as in the simpler case discussed previously; and we add the same caveat.

Among the several inadequacies of the above analysis, the leading one is the neglect of dispersion. This matter is discussed in the following three sections.

Geometrical and Spectral Considerations

As mentioned above and discussed more extensively below, satellite sweep-up holes drift longitudinally at the drift rate of the missing particles. Thus, there is both energy and pitch angle dispersion in the longitudinal drift rate. An idealized instrument measuring several different energy channels at different pitch angles will see holes of various ages at different longitudes and, for a satellite in an eccentric orbit, at different radial locations. Less discriminating detectors observe a superposition of profiles. In principle

our directional detectors A and B have the capability of sorting out the pitch angle dependence of the profile, but the brief period of observation of the microsignature yielded counting rate samples at only a smattering of different pitch angles. For the twelve A and B points which contribute importantly to the establishment of the profile in Figure 4, the pitch angles, in time order, are the following: 139° (41°), 147° (33°), 112° (68°), 121° (59°), 86°, 95° (85°), 60°, 69°, 34°, 43°, 8°, and 18°. The six underlined values are for the most influential points in the vicinity of the minimum of the profile. With one exception (34°) the pitch angles are between 59° and 86°, a fact that will be used later.

The orbit of Mimas is slightly eccentric (e = 0.0215). This feature of the orbit is exploited in the following analysis. According to the best current ephemeris provided us in February 1980 by the Jet Propulsion Laboratory [G. W. Null and J. H. Lieske, personal communication], the radial distance of Mimas varied with time during the Pioneer encounter as shown in Figure 6. At each position Mimas creates absorption holes in the particle population which then drift away at constant r in the magnetic field of the planet to form a locus of holes, continuously moving in longitude. The dipole moment of the planet is taken to be centered and aligned with its rotational axis and of magnitude 0.20 gauss R_s^3 [Smith et al., 1980; Acuna and Ness, 1980]. A spacecraft at a particular radial distance can observe only those holes that were created when the

satellite itself was at that radial distance. Thus, the micro-signature observed at 1546:50.7 ERT at a radial distance of 3.065 R_s must have been created when Mimas was at that radial distance, the most recent such occasion having been at time t = 6.44 hours (2.318×10^4 s) prior to the spacecraft observation (Figure 6). Furthermore, a hole at that radial distance would be present only in those particles that had drifted in 6.44 hours the longitudinal distance between Mimas' position at the earlier time and Pioneer's position at the time of observation. In inertial Saturn-centered equatorial coordinates, this difference in longitude is $\Delta\varphi' = \varphi_p'(1546{:}50.7 \text{ ERT}) - \varphi_M'(0920{:}30 \text{ ERT}) = 49.^{\circ}9$. Electrons whose combined curvature, gradient, and corotation drift would have carried them through this $\Delta\varphi'$ (or $360^{\circ} - \Delta\varphi'$) in 6.44 hours must have had an eastward (+) angular velocity relative to an inertial coordinate system,

$$\omega_I = 3.76 \times 10^{-5} \text{ radian s}^{-1}$$

or a westward (-) angular velocity

$$\omega_I = -2.33 \times 10^{-4} \text{ radian s}^{-1}.$$

Further discrete values of ω_I for particles that have drifted westward by $(720^{\circ} - \Delta\varphi')$, $(1080^{\circ} - \Delta\varphi')$, etc. are mathematically possible but occur for such high energies that they appear to be of no interest, because of the spectral paucity of such particles [Van Allen et al., 1980b].

The angular velocity ω_I of electrons relative to an inertial coordinate system is given by

$$\omega_I = \Omega + \omega_D \qquad (6)$$

where Ω is the angular velocity of the planet (corotation), 1.637×10^{-4} radian s^{-1} [Kaiser et al., 1980], and

$$\omega_D = -2.083 \times 10^{-5} \, L E \left(\frac{E + 1.022}{E + 0.511} \right) \left(\frac{F}{G} \right) \qquad (7)$$
$$[\text{radian } s^{-1}]$$

where E is kinetic energy in MeV, L is the dimensionless magnetic shell parameter and F/G is a weak function of equatorial pitch angle α_o, being 1.0000 for $\alpha_o = 90°$ and 0.9571 for $\alpha_o = 60°$ [Thomsen and Van Allen, 1980].

Using Equations (6) and (7), we find that E = 1.59 MeV for the eastward drifting case and 5.74 MeV for the westward drifting case. For each of these energies we can determine the present location (i.e., at the time of Pioneer's observations) of the holes that Mimas created at various times in the past along its orbit. In Figure 7(a) we show the location at 1546:51 ERT (the time of the observed microsignature) of the locus of holes that Mimas has created in the population of 1.59 MeV electrons during the preceding 18 hours. Each dot is the present location (in radial distance and inertial Saturn-centered longitude) of the hole created by Mimas

(n + 0.3558) hours earlier, where the values of n are shown for every other point. Figure 7(a) also shows the track of Pioneer 11 through Mimas' orbit at a longitude of 307°. (Longitude φ' is measured eastward from the inertial plane passing through the 1950.0 ecliptic pole and Saturn's axis pole, taking the 1950.0 ecliptic/equinox longitude and latitude of the latter to be 78°.8142 and 61°.9324, respectively.) The spacecraft trajectory intersects the locus at $r = 3.065\ R_s$, the location of the observed micro-signature at t = 6.44 hours as required.

Figure 7(b) shows the location at the same time (1546.51 ERT) of the locus of holes that Mimas has created in the population of 5.74 MeV electrons during the preceding 18 hours. As with the 1.59 MeV locus, this one is intersected by the spacecraft trajectory at $r = 3.065\ R_s$, t = 6.44 hours as required. However, there is a more recent point of intersection at $r = 3.032\ R_s$, t = 0.9 hours. This fact shows that if the particles whose shadow is observed at $3.065\ R_s$ have energy E = 5.74 MeV, then we should also have seen another much younger (and therefore deeper) signature at $3.032\ R_s$. As is evident in Figure 1, no such signature was present. Successively higher energies in the discrete set referred to above all have similar younger intersections at radial distances decidedly less than $3.065\ R_s$.

Figures 8(a) and 8(b) show the loci of holes for E = 1.59 MeV and 5.74 MeV, respectively, at the time of Pioneer 11's outbound crossing of Mimas' orbit. As seen in Figure 8(a), there is

no intersection between the spacecraft trajectory and the 1.59 MeV locus for any t less than some tens of hours. We therefore would expect to see no signature in electrons of this energy along the outbound traversal. On the other hand (Figure 8(b)), the 5.74 MeV locus intersects the spacecraft trajectory at $r = 3.036\ R_S$, $t = 4.4$ hours. Unless the fill-in time is considerably shorter than this, we would expect to see a microsignature at that location. But as shown in Figure 1 there is no perceptible microsignature in the outbound data at any point.

Thus, both inbound and outbound observations make it virtually certain that the electrons whose shadow we observe have energies in a narrow spectral range around 1.59 MeV.

A striking feature of Figure 4 is the coherence of the normalized microsignatures from the three detectors. Despite the very different nominal energy thresholds of the detectors [see Van Allen et al., 1980b], all three profiles show a dip to about 65 percent of the ambient level centered at 1546:51. The width of the dip is also very similar for all three detectors. As we have discussed above, particles with different energies drift at different rates relative to the satellite, with the result that a spacecraft should observe holes corresponding to electrons with different energies at different radial distances. Thus, the fact that the microsignature is coherent in our three detectors shows that they are all responding to electrons in the same,

rather narrow energy range. In an accompanying paper [Van Allen et al., 1980b] we have shown on entirely independent grounds that there are essentially no electrons having energies less than an L-dependent value E^*, where $E^* = 1.46$ MeV at Mimas' orbit. Also in the range $10 > L > 5$, our best determination of the differential energy spectrum for $E > E^*$ is of the form $E^{-3.8}$. We have further shown that the response of detectors C and D within the Mimas microsignature region are probably attributable to bremsstrahlung from the same population of electrons that causes the direct responses of detectors A and B. These independent inferences are consistent with the fact that detectors A, B, C (and D) all show time- and space-coherent signatures (Figure 4).

Energy and Pitch Angle Dispersion

The observed absorption signature of a satellite is a superposition of the signatures of components of the particle population having different energies E and equatorial pitch angles α_o. Inasmuch as ω_D (Equation (7)) at a given L is a function of E and of α_o, the signature of a satellite in an eccentric orbit becomes broader in radial width and less deep as the point of observation moves away from the point of origin of the shadow. The nature of this effect is illustrated by Figure 9. At each point along the satellite's path P_1P_2, the satellite "sheds" holes which drift in longitude at constant **r** along lines such as $P_1Q_1Q_1'$ and $P_2Q_2Q_2'$.

In Figure 9, Q_1 is the present (t = 0) position of a hole created in the electron population at E and α_o at the previous time t at which Mimas was at P_1; and Q_1' is the present position of a hole created at E + δE and $\alpha_o + \delta\alpha_o$ at the same previous time. $\overline{Q_1 Q_1'}$ is the resulting dispersion of position. The drifting shadow locus is the cross-hatched strip. As Pioneer 11 cuts through this strip it observes a shadow of slant width $\overline{AB}$. The angle ψ is the arc tangent of the ratio of the radial speed to the circumferential speed of the satellite in its slightly eccentric orbit and the angle ξ is the arc tangent of this ratio for the spacecraft in its hyperbolic encounter trajectory. At the point at which the shadow is observed r = 3.065 R_s, t = 6.44 hr, ψ = 1°.09, and ξ = 50°.4. Inasmuch as the dominant part of the observed shadow lies in the pitch angle range $90 > \alpha_o > 60°$, dispersion in α_o makes a considerably smaller contribution to $\overline{AB}$ than does dispersion in energy. If we take $\overline{AB}$ = 850 km (Figures 2 and 4) we find by differential analysis that the corresponding

$$\delta E \sim 0.1 \text{ MeV} . \qquad (8)$$

Also it is clear that the superposition of overlapping signatures for different energy components of the particle

population produces a shallow composite signature, as observed.

Thus, the principal conclusion of this section is that the breadth of the electron spectrum about its peak at 1.59 MeV can not exceed ~ 0.1 MeV, because this spectral breadth alone accounts for essentially the full radial width of the observed signature without any contribution by diffusion and the finite size of Mimas.

The physical causes of such a nearly monoenergetic spectrum and the implications on the magnitude of the diffusion coefficient are examined in the next section.

Spectral Filtering by Successive Satellites

The characteristics of the spectrum of electrons which are developed by Van Allen et al. [1980b] for $L > 5$ are (a) that there is a low energy cut-off E^* at a given L; (b) that E^* increases with decreasing L as implied by the constant value of the first adiabatic invariant $\mu^* = 525$ MeV/gauss (inbound data), the relationship between E^* and μ^* being as follows for $\alpha_o = 90°$:

$$E^* = 0.511 \left[\left(1 + \frac{2B\mu^*}{0.511}\right)^{\frac{1}{2}} - 1 \right]; \qquad (9)$$

and (c) that the differential energy spectrum for $E > E^*$ is of the form $E^{-3.8}$.

As the net inward diffusion of electrons proceeds the spectrum is subjected to the filtering effect of absorption by the succession of satellites -- Rhea, Dione, Tethys, and Enceladus -- outside of Mimas' orbit. Each of these satellites acts as a spectral band-pass filter, favoring the survival of electrons having energies such that

$$\omega_I = \omega_K \qquad (10)$$

where ω_K is the Keplerian angular velocity of the satellite. Such favored electrons are the so-called resonant or synchronous ones, for which the interval between successive encounters with the satellite $2\pi/(|\omega_I - \omega_K|)$ is infinite. Electrons of the appropriate energy diffuse across a satellite's orbit as though the satellite were not there, whereas electrons having

off-resonant energy are subjected to losses. Table 1 lists the resonant energies from Thomsen and Van Allen [1980]. The sequence of satellites imposes a series of overlapping band-pass filters on the spectrum of inward diffusing electrons. The full problem has not yet been solved. But because of the presumed rapid increase of the diffusion coefficient D with increasing L, the filtering effect of the next outer satellite from Mimas, namely Enceladus, is likely to be the most influential in conditioning the spectrum of electrons arriving at Mimas' orbit. In Figure 10, the time interval between successive encounters of an electron with Enceladus is shown as a function of energy for α_o = 30° and 90°. (Of incidental interest here is the dramatic difference between the curves for electrons and protons as shown in Figure 10.) As an example, electrons having α_o = 90° and resonant energy E = 1.00 MeV at Enceladus arrive at Mimas, if the first two adiabatic invariants (μ = 620 MeV/gauss, J = 0) are conserved, with E = 1.62 MeV, a value remarkably close to the dominant energy (1.59 MeV) that we have inferred on an altogether independent basis from the microsignature analysis in previous sections. Moreover, the spectrum of surviving electrons at Mimas can have the above inferred nearly-monoenergetic form ($\delta E \sim 0.1$ MeV) if the characteristic diffusion time across Enceladus' orbit is such as illustrated by the horizontal line AA' in Figure 10. Adopting τ = 5 (cf. Figure 5), taking $t = 3 \times 10^5$ s from Figure 10, and $b = 3.0 \times 10^7$ cm [Cruikshank, 1978], we find from Equation (2) that

$$D \sim 1.0 \times 10^{-10} R_s^2 \ s^{-1} \qquad (11)$$

at L = 4 for electrons of kinetic energy E = 1 MeV. This value of D is one of the principal results of the present paper. It is thought to be valid to within a factor of 2. At Mimas (L = 3.092), D will presumably be less by the factor $(3.092/3.968)^m$ where m is the index of a power law dependence of D on L; for m = 4, D at L = 3 would be $3.7 \times 10^{-11} R_s^2 \ s^{-1}$; and for m = 10, D at L = 3 would be $8.3 \times 10^{-12} R_s^2 \ s^{-1}$. Either of these values of D is consistent with our earlier conclusion that the profile of the observed microsignature is attributable primarily to energy dispersion and not to radial diffusion. Also, it is evident that the width of the observed profile is insensitive to the radius of the causative satellite and, therefore, does not yield a significant determination of b.

Summary

Data are presented for a one-minute dip in electron intensity that was observed coherently by four different University of Iowa detectors at 1546:51 ERT on DOY 244/1979 as Pioneer 11 crossed the orbit of Mimas inbound during its encounter with the Saturn system. By a detailed analysis, we show that (a) this absorption microsignature in electron intensity is plausibly attributable to the particle sweeping effect of Mimas; (b) the radial width of the signature is caused primarily by energy dispersion in the

longitudinal drift rate of electrons and not by radial diffusion; (c) the spectrum of trapped electrons at Mimas is nearly monoenergetic, centered at kinetic energy E = 1.59 MeV with a spread $\delta E \sim 0.1$ MeV; (d) this narrow spectrum, which is unique in magnetospheric physics, is caused by the "band-pass filtering" action of the successive inner satellites, most importantly Enceladus, on an inward diffusing population of electrons; and (e) the radial diffusion coefficient D of electrons E = 1.0 MeV is $1.0 \times 10^{-10} R_s^2 s^{-1}$ at L = 4 and probably in the range 3.7×10^{-11} to $8.3 \times 10^{-12} R_s^2 s^{-1}$ at L = 3.

Discussion

Our analysis proceeds from the basic hypothesis that the observed microsignature is attributable to Mimas. Thereafter it is straightforward and free of ad hoc assumptions. The results are insensitive to mild departures of the true magnetic field from the centered, untilted dipolar model of Saturn's magnetic field that we adopted as being consistent with present knowledge. A dipolar tilt of 1° - 2° to the rotational axis of the planet has a negligible effect on the conclusions and an equatorial offset of 0.01 R_s, the largest value permitted by present knowledge [Simpson et al., 1980b], has only a mild effect.

In view of the internal consistency of our analysis as demonstrated above, we find a puzzling feature of the whole body of data on the microsignature to be the fact that it was observed, and indeed discovered, by the University of Chicago

group with detectors of quite different nominal characteristics. Figure 3 of Simpson et al. [1980a] shows the microsignature in a detector channel labelled "Electrons 7 - 17 MeV" and also (though with slightly poorer statistics) in a channel labelled "Protons 0.5 - 1.8 MeV". These two microsignatures occur in accurate temporal coincidence with each other and with the signature observed by the Iowa detectors (i.e., at the same radial distance); also, all five of the microsignatures are of similar depth. Yet we have shown that shadows for particles of different species and energy must appear at different radial distances, if such shadows are indeed caused by Mimas. A possible basis for reconciliation lies in the difficult problem of identification of the species and energy of particles causing the responses of the several detectors of the Iowa and Chicago instruments under the stringent radiation conditions in Saturn's inner magnetosphere. A critical discussion of the responses of the Iowa detectors within this region is given in Appendices A and B of Van Allen et al. [1980b]. In view of the large geometric factors and slow electronics (≥ 2 μs) of the Chicago instrument and of its low counting rates in the Mimas region, we find it difficult to accept at face value the nominal identification of the particle species and energies causing the responses of these detectors in the presence of an omnidirectional intensity 4.4×10^6 $(cm^2\ sec)^{-1}$ of electrons of $\sim$ 1.6 MeV. We think it more likely that the

two Chicago detectors are also responding primarily, in this region, to the same population of electrons that we have identified. If this is true, the Iowa and Chicago results are consistent with each other and with our Mimas interpretation of the microsignature.

If, on the other hand, the particles responsible for the Chicago detectors' responses have been correctly identified by Simpson et al. [1980a], there appears to be no choice but to make the ad hoc hypothesis that the microsignature is attributable not to Mimas but to the direct traversal of the magnetic flux tube of another, previously unknown, object trailing Mimas in a similar orbit by a longitude difference of about 56°. The approximate equality of this longitude difference with the 60° for the trailing triangular Lagrangian point (L5) of the Mimas-Saturn system has led Dermott et al. [1980] and Simpson et al. [1980b] to advocate this hypothesis. In considering this suggestion, it must be noted that protons E_p = 1 MeV at L = 3.09 and equatorial pitch angle 90° drift eastward at an angular velocity of 2.2×10^{-4} radian s^{-1} whereas electrons E_e = 10 MeV drift westward at an angular velocity of 5.9×10^{-4} radian s^{-1}, both referenced to a satellite in a circular Keplerian orbit. Inasmuch as the two Chicago microsignatures and the three Iowa microsignatures were accurately coincident in time (and space), this line of interpretation requires acceptance of an exceedingly unlikely coincidence, namely that Pioneer 11

passed almost exactly through the center of the circular magnetic flux tube containing the hypothetical satellite. Also it requires quantitative justification for the absence of a Mimas microsignature. In addition, we consider that there are specific objections as follows. The prime example of a microsignature in the Saturn encounter data of Pioneer 11 is the discovery signature of satellite 1979 S2 at 2.534 R_s [Van Allen et al., 1980a]. The absorption was nearly 100 percent at the center of this signature and its width was ~ 170 km. At this position the trapped particle population is of similar nature to that at Mimas' orbit. Absorption profiles in "7 - 17 MeV electrons" and "0.5 - 1.8 MeV protons" were also found by the Chicago group in this case and because of the constraint imposed by their particle identification, they were compelled to propose a nearly exact flux tube traversal. We did not and do not join in this constraint and can easily accommodate a miss in longitude of several degrees or more to the west of the satellite.

In the case at hand, we may reiterate the analogous objection as follows. If coincident absorption signatures are observed by two different detectors that are truly sensitive to two different classes of particles whose longitudinal drifts relative to the absorbing body are in opposite senses, then a flux tube traversal is a necessary conclusion, unlikely as such an occurrence may be. If, however, irrespective of the nominal characteristics of the detectors they are actually responding to the same class of

particles, no such conclusion is justified (though it might be true fortuitously). In this second possibility, the absorption shadow may stretch out from the satellite over many degrees of longitude if energy dispersion and diffusive fill-in are sufficiently gradual.

Further evidence against the hypothesis of direct flux tube traversal in the case at hand is the fact that the observed absorption is only about 20 to 40 percent, suggesting considerable fill-in, i.e., "old" signatures. (Contrast with the 98 percent absorption for the signature of 1979 S2.) Also it may be noted that the radial width of the microsignature at half-absorption is ~ 680 km (Figures 2 and 4). If this were a "fresh" signature (i.e., one which had suffered very little diffusive or dispersive fill-in but which, for some unknown reason, exhibited much less than 100 percent absorption) the responsible body would be comparable to Mimas in size and would have been discovered by ground based astronomers many years ago. Even if an alternative ad hoc hypothesis of a cluster or cloud of many small satellites near the L5 Lagrangian point were put forward, it would be difficult if not impossible to account for the observed particle absorption without violating the absence of prior optical evidence.

Thus, even apart from consideration of the technical details of detectors, we find it very unlikely that the Chicago group's identification of the particles causing the responses of their two relevant detectors can be correct in the Mimas region of Saturn's magnetosphere.

For all of the reasons given above we continue to favor the Mimas interpretation of the absorption microsignature observed by Pioneer 11 at r = 3.065 inbound. A corollary aspect of this position is that the whole body of relevant particle data neither proves nor disproves the possibility of one or more small satellites at or near the L5 point of the Mimas-Saturn system.

We have made a preliminary inquiry into the reason that microsignatures of Enceladus, Tethys, Dione, and Rhea were not observed. Within the context of this paper, it appears likely that increases in spectral spread and energy dispersion and, probably, in D with increasing L are responsible for these negative findings.

Acknowledgements

We thank E. D. Robison, R. L. Rairden, and C. L. Grosskreutz for assistance with various aspects of the work and G. W. Null and J. H. Lieske of the Jet Propulsion Laboratory for the best available ephemeris of Mimas. We are grateful to two referees who criticized earlier versions of this paper and especially to Referee A. W. Schardt of the Goddard Space Flight Center/NASA who urged us to develop a more quantitative treatment of the band-pass filtering effect of Enceladus and to improve our discussion of energy and pitch-angle dispersion. This research was supported in part by the Ames Research Center/NASA under contract NAS2-6553 and by the U. S. Office of Naval Research.

REFERENCES

Acuna, M. H., and N. F. Ness, The magnetic field of Saturn: Pioneer 11 observations, Science, 207, 444, 1980.

Cruikshank, D. P., Physical properties of the satellites of Saturn, in The Saturn System, edited by D. M. Hunten and D. Morrison, NASA Publication CP-2068, National Aeronautics and Space Administration, Washington, D. C., 1978.

Dermott, S. F., C. D. Murray, and A. T. Sinclair, The narrow rings of Jupiter, Saturn and Uranus, Nature, 284, 309, 1980.

Fillius, W., W. H. Ip, and C. D. McIlwain, Trapped radiation belts of Saturn: First look, Science, 207, 425, 1980.

Hess, W. N., T. J. Birmingham, and G. D. Mead, Jupiter's radiation belts: Can Pioneer 10 survive?, Science, 182, 1021, 1973.

Hess, W. N., T. J. Birmingham, and G. D. Mead, Absorption of trapped particles by Jupiter's moons, J. Geophys. Res., 79, 2877, 1974.

Jacques, S. A., and L. Davis, Diffusion models for Jupiter's radiation belt, Cal. Inst. of Tech. Report, Pasadena, CA, 1972.

Mead, G. D., Effect of Jupiter's satellites on the diffusion of protons, Proc. Jup. Rad. Belt Workshop, JPL Tech. Mem. 33-543, 271, 1972.

Mead, G. D., and W. N. Hess, Jupiter's radiation belts and the sweeping effects of its satellites, J. Geophys. Res., 78, 2793, 1973.

Mogro-Campero, A., Absorption of radiation belt particles by the inner satellites of Jupiter, in Jupiter, edited by T. Gehrels, p. 1190, University of Arizona Press, Tucson, 1976.

Mogro-Campero, A., and R. W. Fillius, The radial diffusion coefficient of particle transport in the inner magnetosphere of Jupiter, EOS Trans. Am. Geophys. Union, 55, 1172, 1974.

Mogro-Campero, A., and R. W. Fillius, The absorption of trapped particles by the inner satellites of Jupiter and the radial diffusion coefficient of particle transport, J. Geophys. Res., 81, 1289, 1976.

Simpson, J. A., D. C. Hamilton, R. B. McKibben, A. Mogro-Campero, K. R. Pyle, and A. J. Tuzzolino, The protons and electrons trapped in the Jovian dipole magnetic field region and their interaction with Io, J. Geophys. Res., 79, 3522, 1974.

Simpson, J. A., T. S. Bastian, D. L. Chenette, G. A. Lentz, R. B. McKibben, K. R. Pyle, and A. J. Tuzzolino, Saturnian trapped radiation and its absorption by satellites and rings: The first results from Pioneer 11, Science, 207, 411, 1980a.

Simpson, J. A., T. S. Bastian, D. L. Chenette, R. B. McKibben, and K. R. Pyle, The trapped radiations of Saturn and their absorption by satellites and rings, J. Geophys. Res., 85, this issue, 1980b.

Smith, E. J., L. Davis, Jr., D. E. Jones, P. J. Coleman, Jr., D. S. Colburn, P. Dyal, and C. P. Sonett, Saturn's magnetic field and magnetosphere, Science, 207, 407, 1980.

Thomsen, M. F., Determination of the electron diffusion coefficient from observed Jovian satellite sweep-up effects, EOS Trans. Am. Geophys. Union, 57, 316, 1976.

Thomsen, M. F., On determining a radial diffusion coefficient from the observed effects of Jupiter's satellites, Ph.D. thesis, University of Iowa, Iowa City, 1977.

Thomsen, M. F., Jovian magnetosphere-satellite interactions: Aspects of energetic charged particle loss, Rev. Geophys. Space Phys., 17, 369, 1979.

Thomsen, M. F., and C. K. Goertz, Satellite sweep-up effects at Jupiter, EOS Trans. Am. Geophys. Union, 56, 428, 1975.

Thomsen, M. F., C. K. Goertz, and J. A. Van Allen, On determining magnetospheric diffusion coefficients from the observed effects of Jupiter's satellite Io, J. Geophys. Res., 82, 5541, 1977a.

Thomsen, M. F., C. K. Goertz, and J. A. Van Allen, A determination of the L dependence of the radial diffusion coefficient for protons in Jupiter's inner magnetosphere, J. Geophys. Res., 82, 3655, 1977b.

Thomsen, M. F., and J. A. Van Allen, Motion of trapped electrons and protons in Saturn's inner magnetosphere (with extensive tables), University of Iowa 80-25, July 1980 and J. Geophys. Res., 85, this issue, 1980 (with abridged tables).

Trainor, J. H., F. B. McDonald, and A. W. Schardt, Observations of energetic ions and electrons in Saturn's magnetosphere, Science, 207, 421, 1980.

Van Allen, J. A., M. F. Thomsen, B. A. Randall, R. L. Rairden, and C. L. Grosskreutz, Saturn's magnetosphere, rings, and inner satellites, Science, 207, 415, 1980a.

Van Allen, J. A., B. A. Randall, and M. F. Thomsen, Sources and sinks of energetic electrons and protons in Saturn's magnetosphere, J. Geophys. Res., 85, this issue, 1980b.

Table 1

Resonant Electron Energies at the Orbits of Five Satellites of Saturn

Satellite	Semi-major axis, R_S	Resonant Energy, MeV		
		α_o = 30°	60°	90°
Rhea	8.787	0.66	0.57	0.54
Dione	6.292	0.90	0.78	0.74
Tethys	4.913	1.09	0.94	0.90
Enceladus	3.968	1.21	1.05	1.00
Mimas	3.092	1.22	1.06	1.00

FIGURE CAPTIONS

Figure 1. Counting rates of University of Iowa detectors A, B, C, and D during the inbound and outbound traversals of the region of Mimas' orbit. Lighter curves show data at the finest time resolution available, and heavier curves show 14 sample (115.5 second) averages. The horizontal bar labeled Mimas shows its excursion in radial distance as it moves in its slightly eccentric orbit.

Figure 2. The normalized profile of the microsignature as given by the counting rate of detector C only. Statistical standard deviations ($\pm \sigma$) of individual counting rate samples are shown by the vertical bars. The solid line is a diffusion fit with parameters as given in the text.

Figure 3. Pitch angle distribution of counting rate of detector B for four minutes of data immediately following the time interval during which the microsignature was observed. The solid line shows an empirical fit to the data. This shape (but not the absolute intensity) was found also to represent quite well the data obtained just prior to the microsignature.

Figure 4. Normalized profile of the microsignature in detectors A, B, and C obtained as described in the text. The solid line is the best fit result of a simple one-dimensional diffusion model of the satellite sweep-up and refilling process for the case of total initial absorption and a particle gyroradius of ρ = 10 km. The diameter of the satellite d = 2b = 180 km and the value of τ are results of the best fit.

Figure 5. An instructive family of curves resulting from the solution of the one-dimensional diffusion equation. Analytical details are specified on the figure.

Figure 6. Radial distance of Mimas as a function of time during the Pioneer 11 encounter with Saturn. At the mid-time of the microsignature (1546:50.7 ERT) the spacecraft was at a radial distance of 3.065 R_s. (The inward radial component of the velocity of the spacecraft was 0.0169 R_s per minute.) At the same time Mimas was at a radial distance of 3.040 R_s and 56°3 eastward of the spacecraft in Saturn-centered inertial coordinates. The latest previous time at which Mimas was at 3.065 R_s was 0920:30 ERT; at that time it was 49°9 westward of the position of the spacecraft at 1546:50.7 ERT (Ephemeris of Mimas, courtesy of G. W. Null and J. H. Lieske of JPL).

Figure 7. Location (radial distance and inertial equatorial Saturn-centered longitude), at the time of the inbound Pioneer observations, of the shadow locus created by Mimas in the population of (a) 1.59 MeV and (b) 5.74 MeV electrons during the preceding 18 hours.

Figure 8(a) and (b). Same as Figure 7(a) and (b), respectively, except at the time of the outbound observations.

Figure 9. A diagram (not to scale) to illustrate the observed width of Mimas' particle shadow caused by energy and pitch angle dispersion in longitudinal drift rates.

Figure 10. Plots of the calculated time interval between successive encounters of electrons (upper two curves) and protons (lower two curves) with Enceladus as a function of kinetic energy of the particles. Of particular interest is the resonant, or synchronous, energy for electrons, E_e = 1.00 MeV for $\alpha_o = 90°$ and E_e = 1.21 MeV for $\alpha_o = 30°$. Protons exhibit no such resonance at any energy. The horizontal line AA′ illustrates a sample diffusion time past Enceladus such as to result in a narrow band-pass filtering effect on the spectrum of electrons diffusing inward across its orbit.

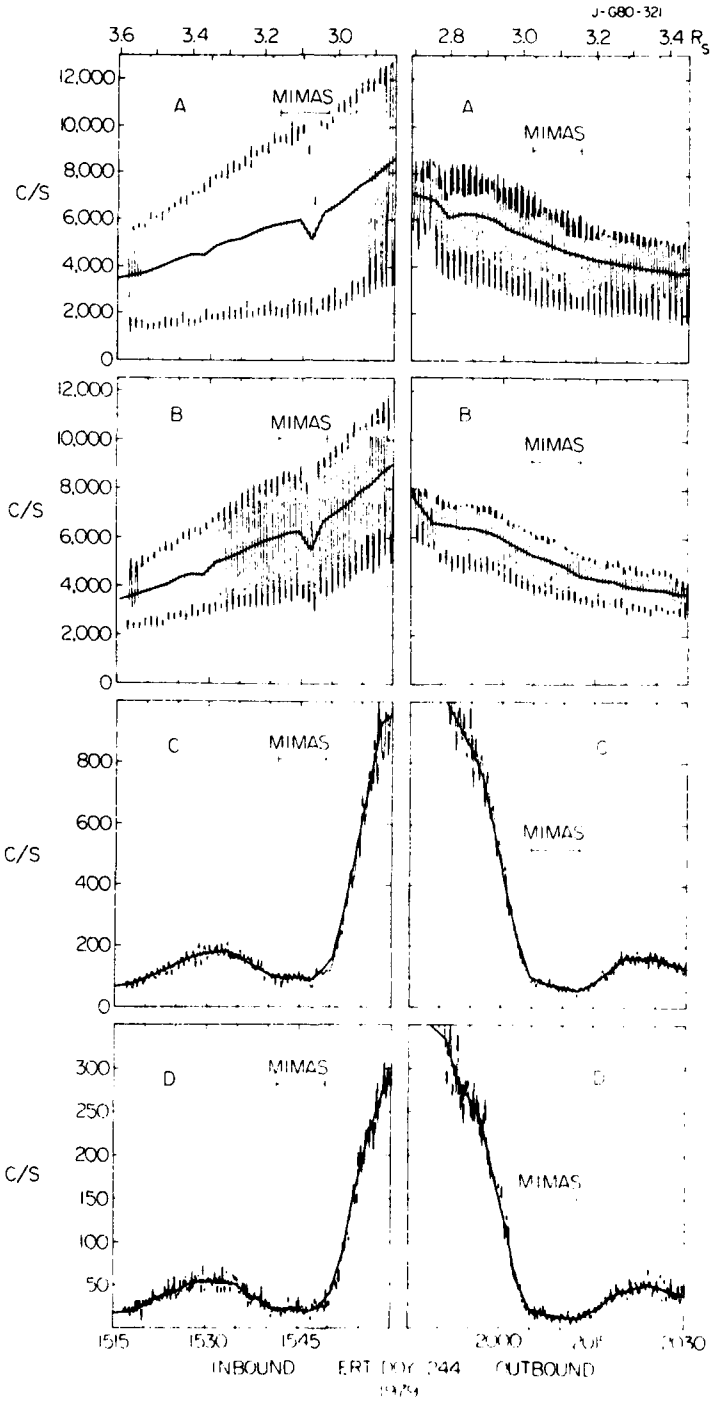
J-G80-321
3.6
3.4
3.2
3.0
2.8
3.0
3.2
3.4 R_S
A
MIMAS
B
MIMAS
C
MIMAS
D
MIMAS
C/S
12,000
10,000
8,000
6,000
4,000
2,000
0
800
600
400
200
300
250
200
150
100
50
1515
1530
1545
2000
2030
INBOUND
OUTBOUND

Figure 1

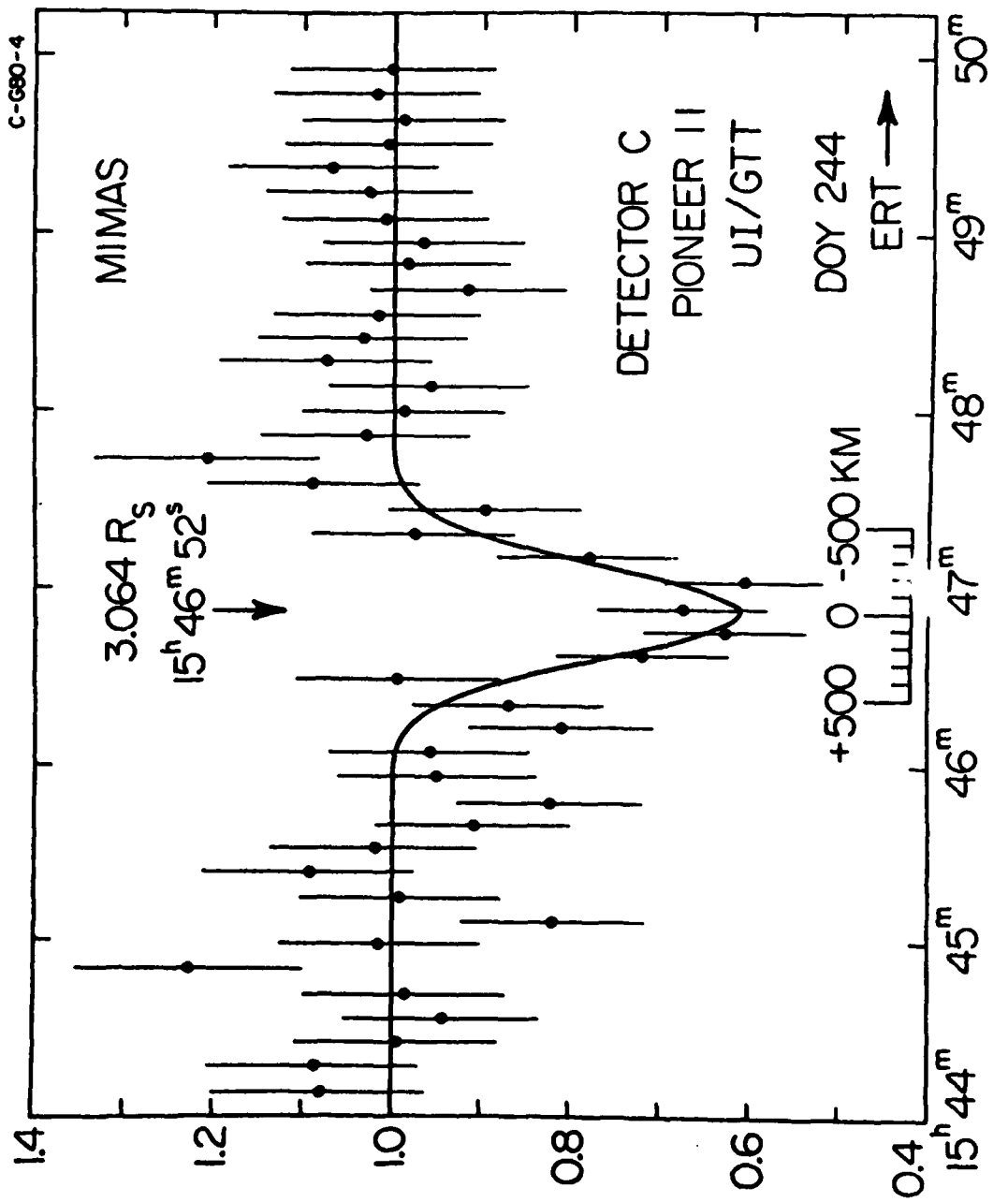
C-G80-4
MIMAS
3.064 R_S
$15^h 46^m 52^s$
DETECTOR C
PIONEER 11
UI/GTT
DOY 244
ERT
+500 0 -500 KM
1.4
1.2
1.0
0.8
0.6
0.4
$15^h 44^m$
45^m
46^m
47^m
48^m
49^m
50^m

Figure 2

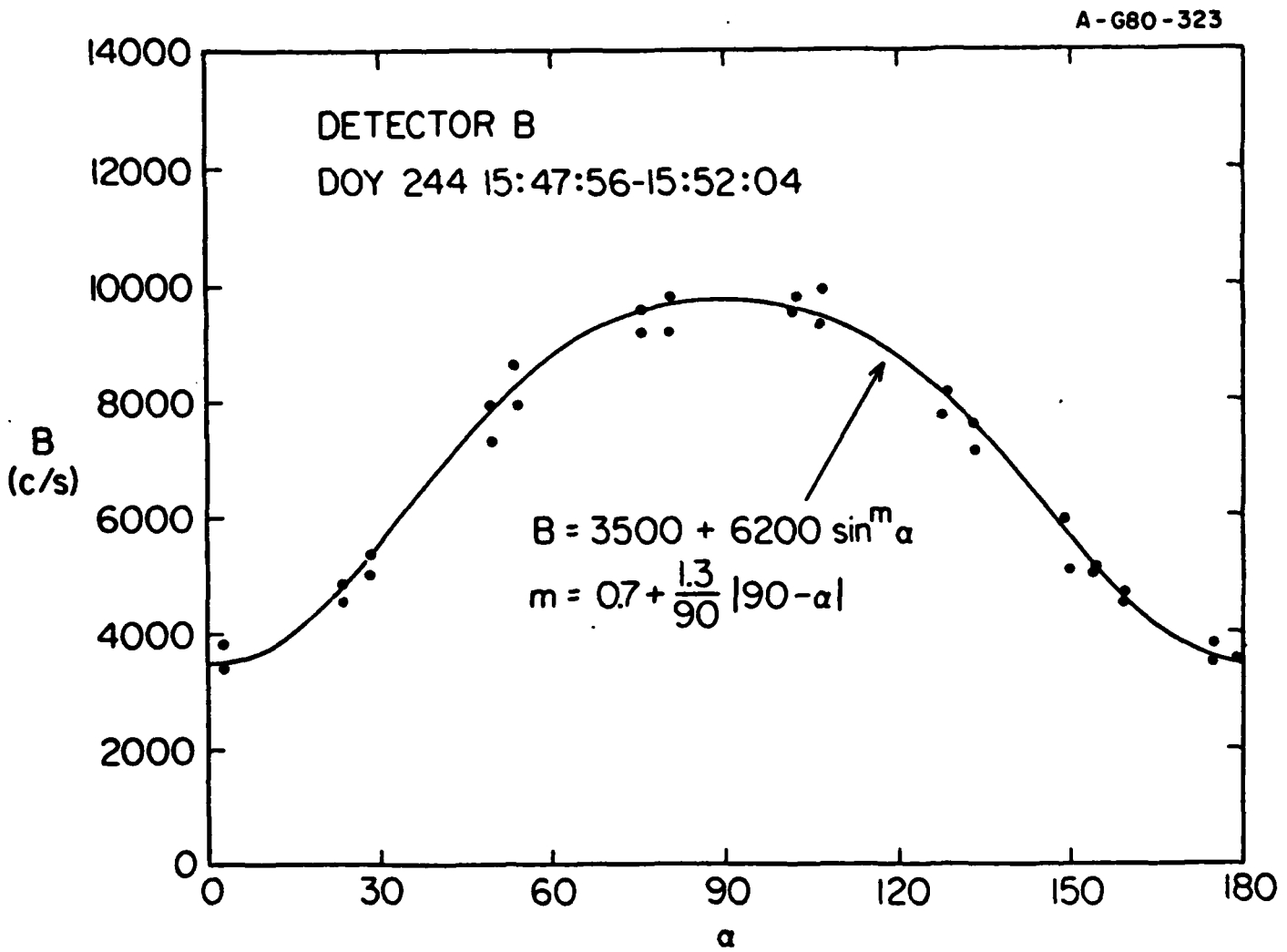
A-G80-323
DETECTOR B
DOY 244 15:47:56-15:52:04
B = 3500 + 6200 sin^m α
m = 0.7 + 1.3/90 |90-α|
B (c/s)
α
0
2000
4000
6000
8000
10000
12000
14000
0
30
60
90
120
150
180

Figure 3

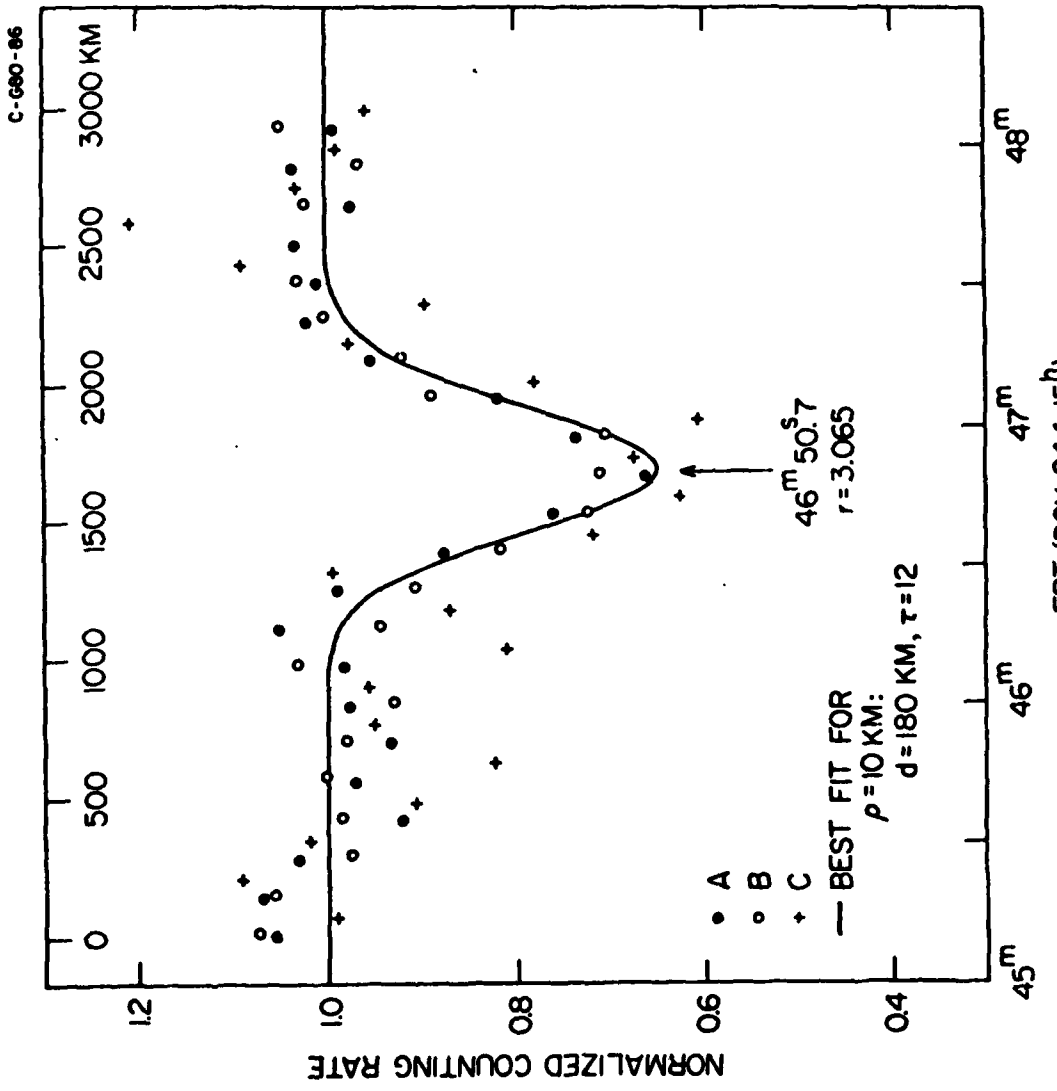
C-680-86
0
500
1000
1500
2000
2500
3000 KM
1.2
1.0
0.8
0.6
0.4
NORMALIZED COUNTING RATE
45m
46m
47m
48m
ERT (DOY 244 15h)
A
B
C
BEST FIT FOR
ρ = 10 KM:
d = 180 KM, τ = 12
46m 50s.7
r = 3.065

Figure 4

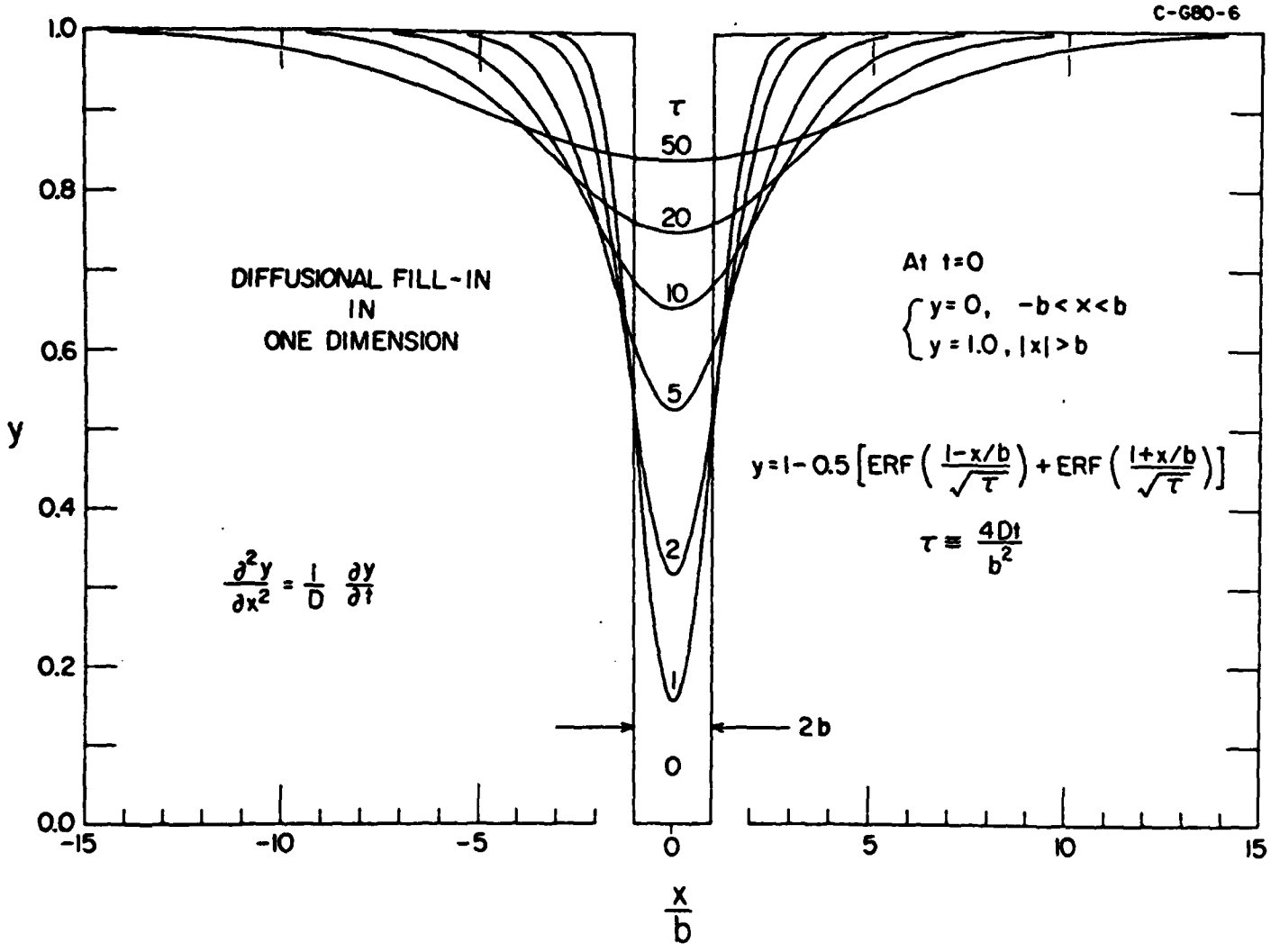
C-G80-6
DIFFUSIONAL FILL-IN
IN
ONE DIMENSION
$\frac{\partial^2 y}{\partial x^2} = \frac{1}{D}\frac{\partial y}{\partial t}$
At t=0
$\begin{cases} y=0, & -b<x<b \\ y=1.0, & |x|>b \end{cases}$
$y = 1 - 0.5\left[\mathrm{ERF}\left(\frac{1-x/b}{\sqrt{\tau}}\right) + \mathrm{ERF}\left(\frac{1+x/b}{\sqrt{\tau}}\right)\right]$
$\tau \equiv \frac{4Dt}{b^2}$
τ
50
20
10
5
2
1
0
2b
y
x/b
1.0
0.8
0.6
0.4
0.2
0.0
-15
-10
-5
0
5
10
15

Figure 5

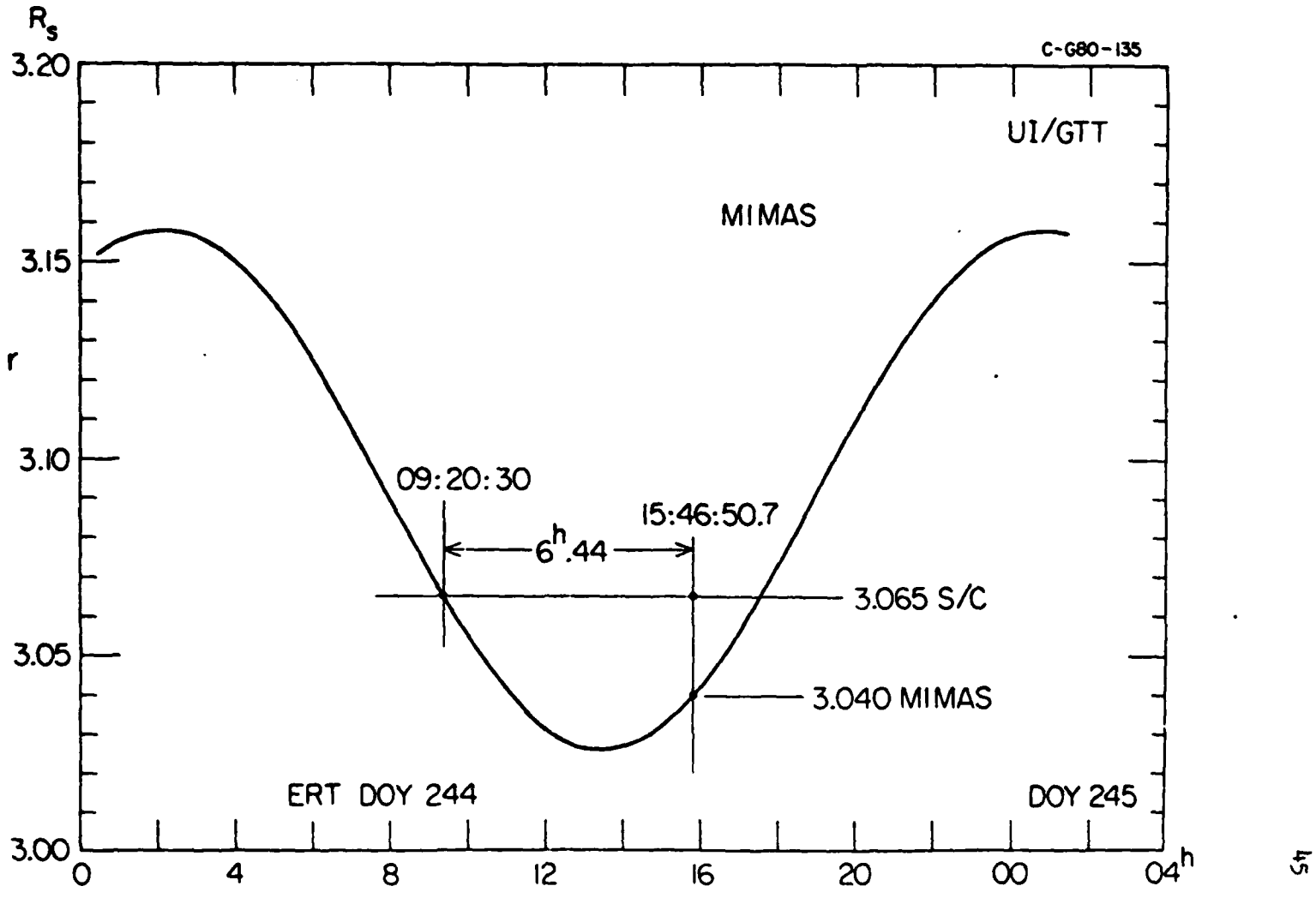
R_s
C-G80-135
3.20
UI/GTT
MIMAS
3.15
r
3.10
09:20:30
15:46:50.7
6^h.44
3.065 S/C
3.05
3.040 MIMAS
ERT DOY 244
DOY 245
3.00
0
4
8
12
16
20
00
04^h

Figure 6

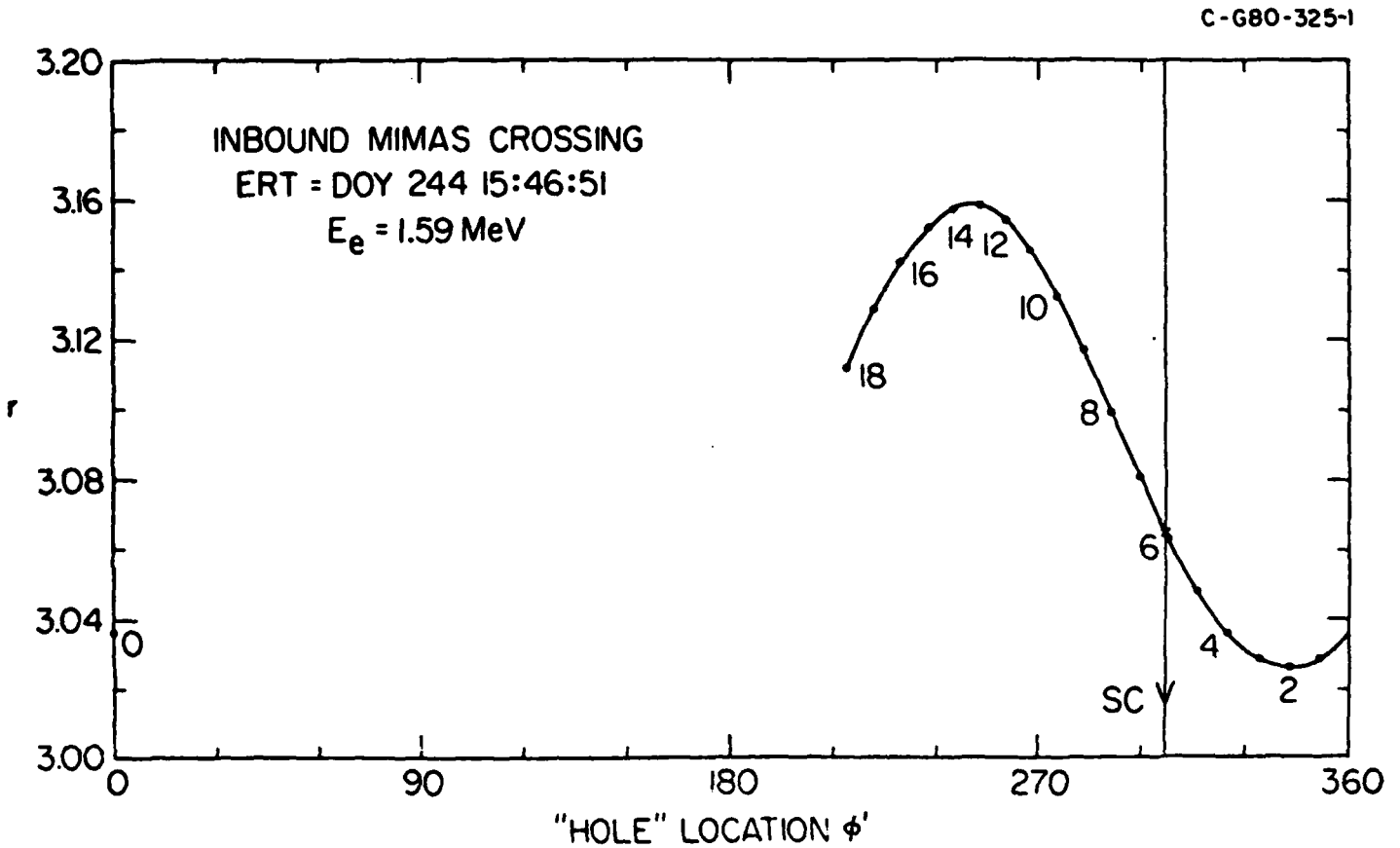
C-G80-325-1
INBOUND MIMAS CROSSING
ERT = DOY 244 15:46:51
E_e = 1.59 MeV
3.20
3.16
3.12
3.08
3.04
3.00
r
0
90
180
270
360
"HOLE" LOCATION φ'
18
16
14
12
10
8
6
4
2
0
SC

Figure 7(a)

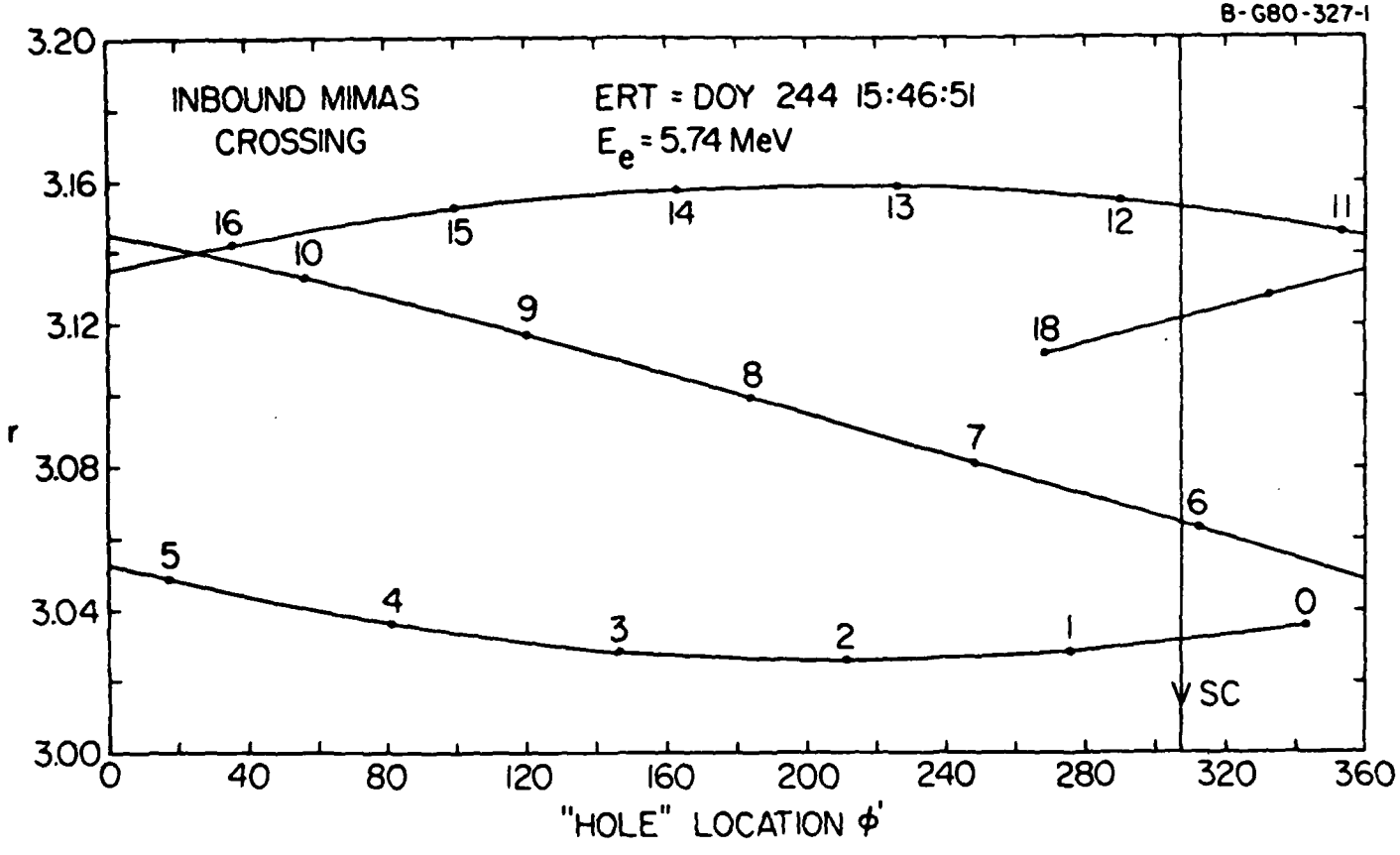
B-G80-327-1
INBOUND MIMAS CROSSING
ERT = DOY 244 15:46:51
E_e = 5.74 MeV
3.20
3.16
3.12
3.08
3.04
3.00
r
0
40
80
120
160
200
240
280
320
360
"HOLE" LOCATION φ'
SC
16
10
15
14
13
12
11
9
18
8
7
6
5
4
3
2
1
0

Figure 7(b)

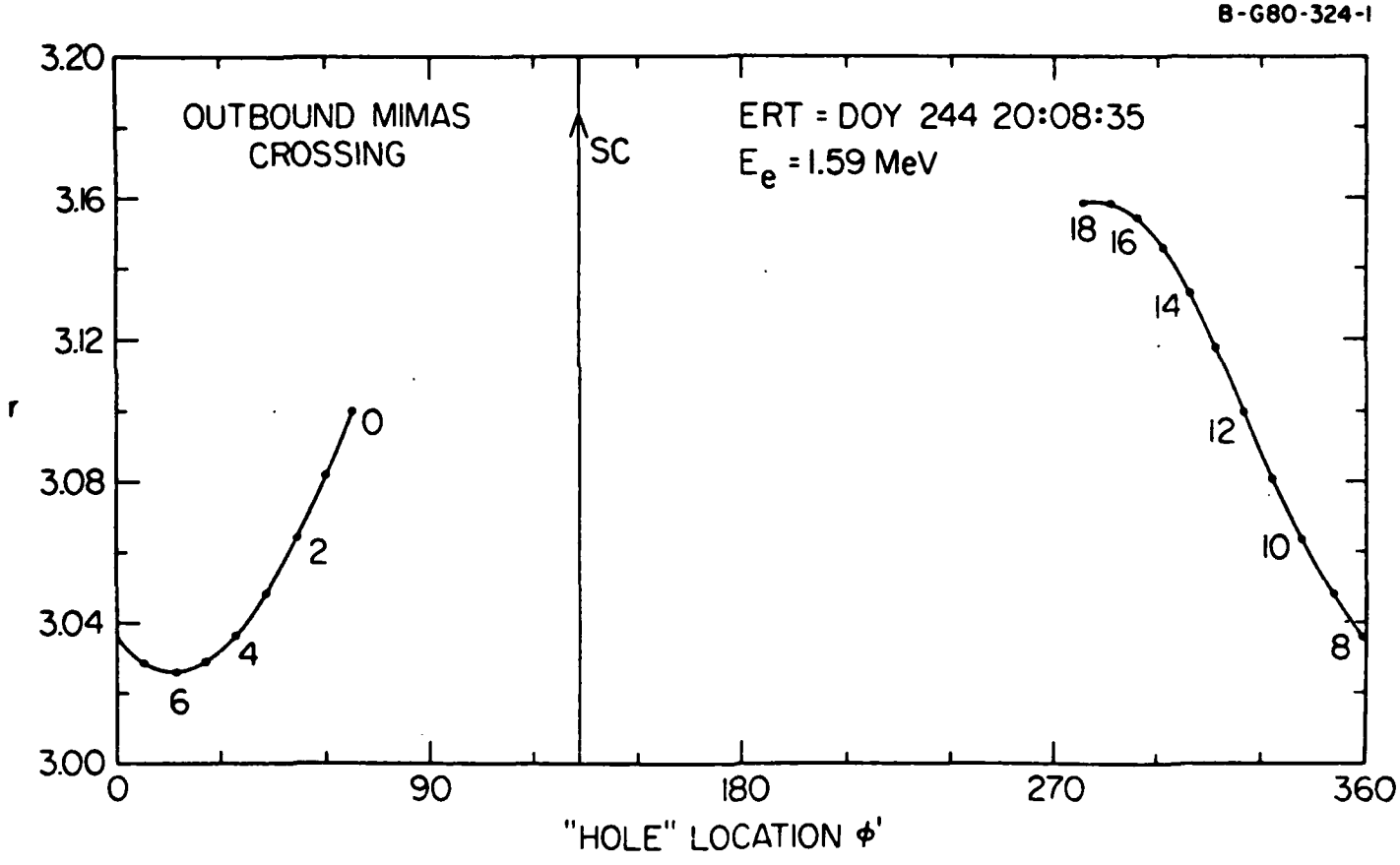
B-G80-324-1
OUTBOUND MIMAS
CROSSING
SC
ERT = DOY 244 20:08:35
E_e = 1.59 MeV
3.20
3.16
3.12
3.08
3.04
3.00
r
0
2
4
6
8
10
12
14
16
18
0
90
180
270
360
"HOLE" LOCATION φ'

Figure 8(a)

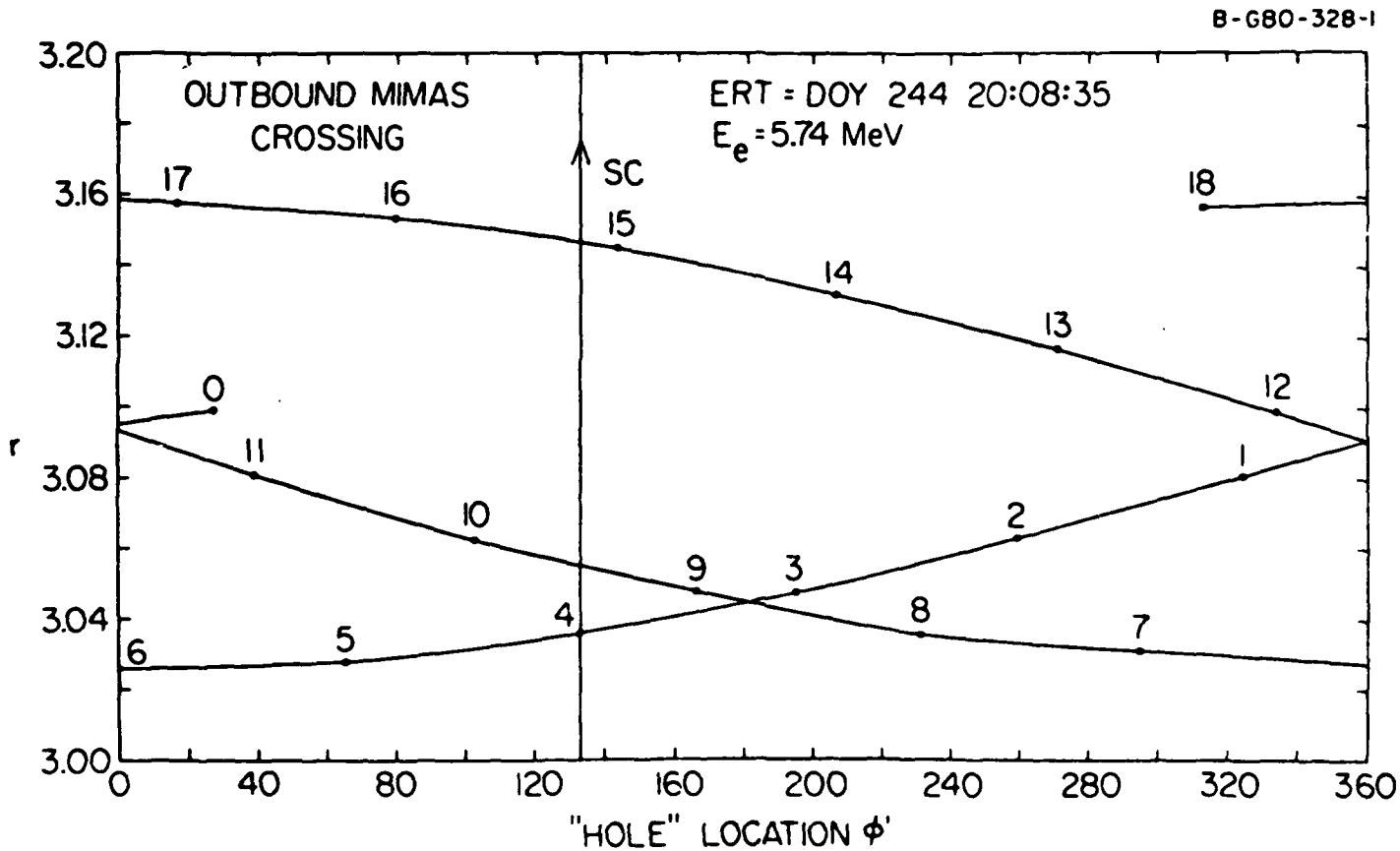
B-G80-328-1
OUTBOUND MIMAS
CROSSING
ERT = DOY 244 20:08:35
E_e = 5.74 MeV
SC
r
3.20
3.16
3.12
3.08
3.04
3.00
0
40
80
120
160
200
240
280
320
360
"HOLE" LOCATION Φ'
17
16
15
14
13
12
18
0
11
10
9
3
2
1
4
8
7
6
5

Figure 8(b)

A-G80-595

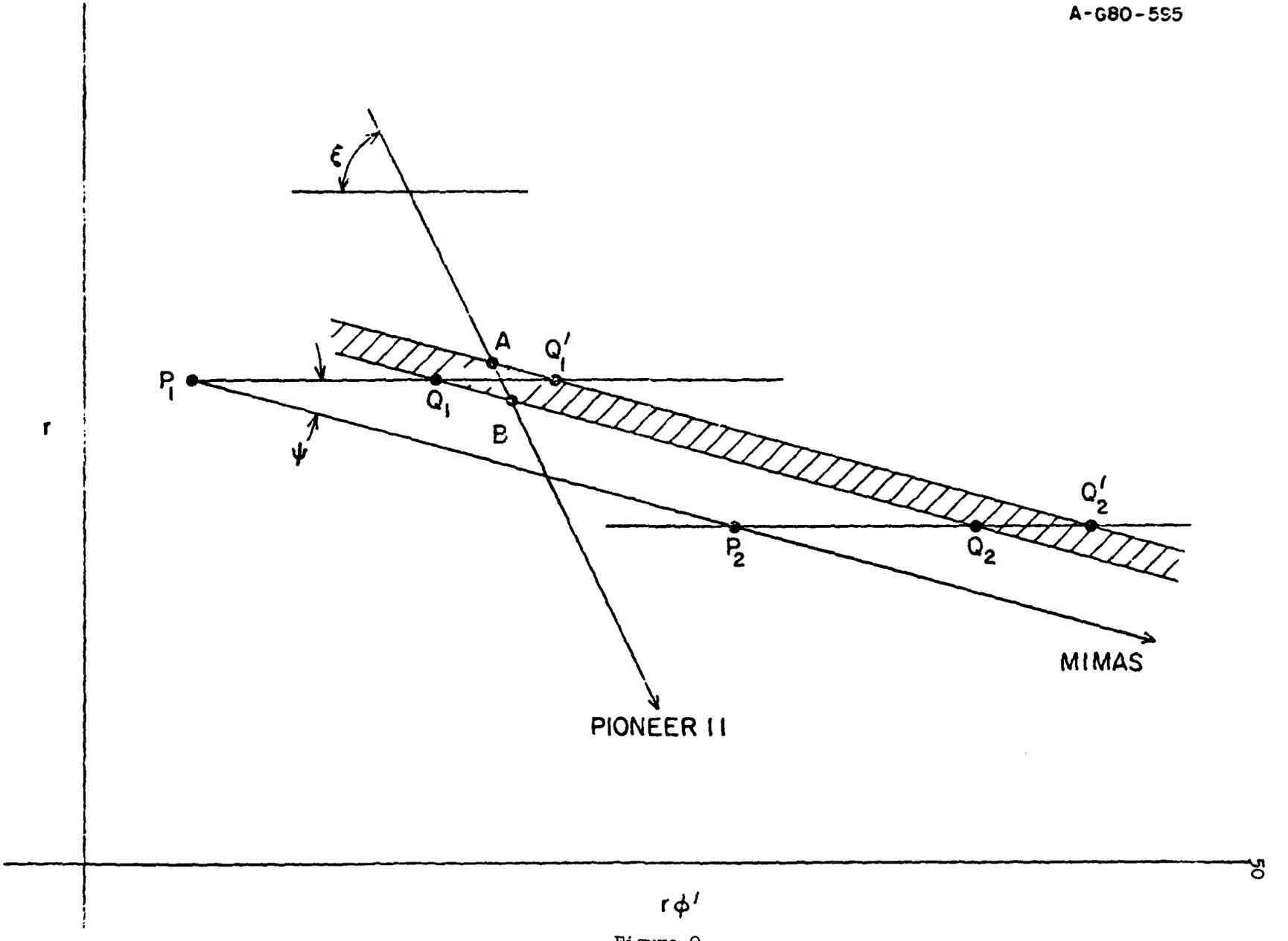

Figure 9

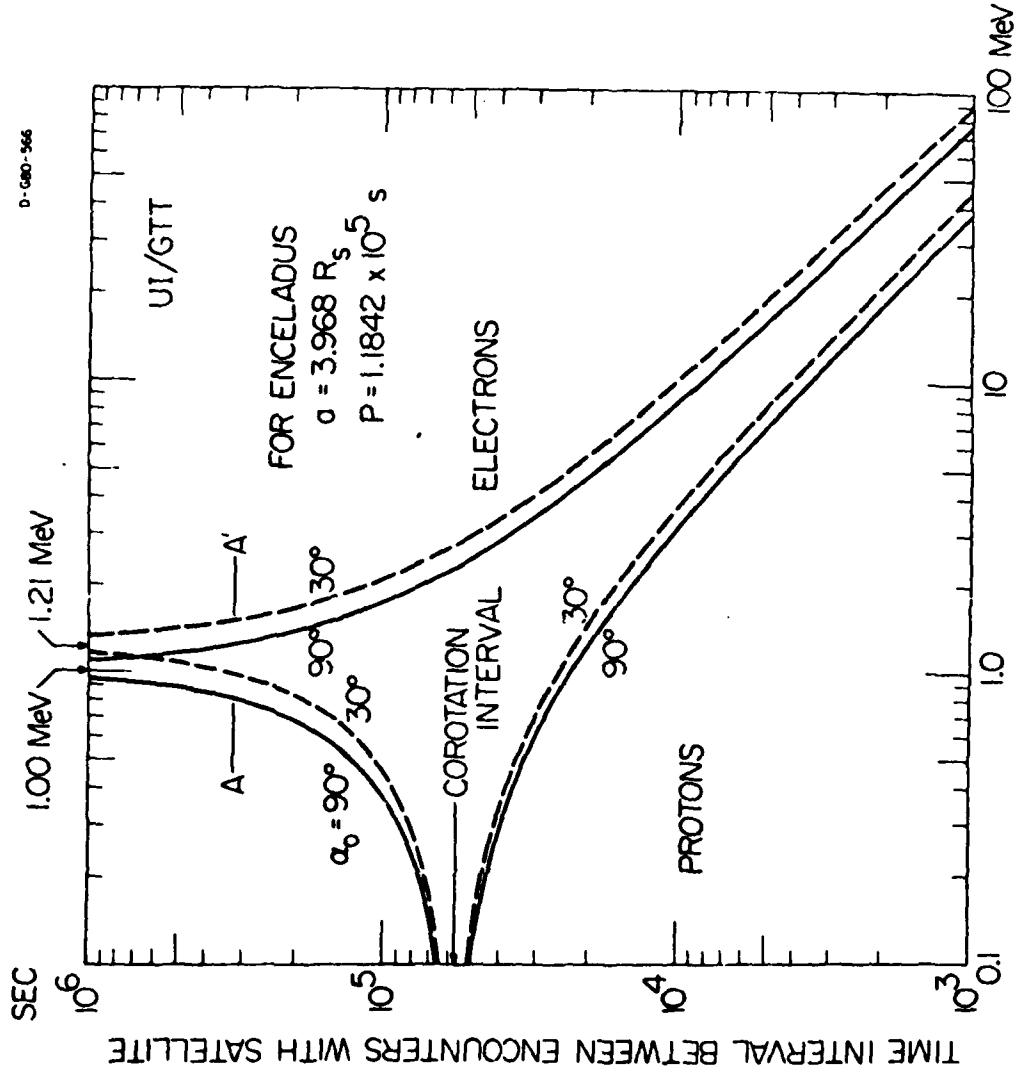
D-GBD-566
U1/GTT
FOR ENCELADUS
a = 3.968 R_s
P = 1.1842 x 10^5 s
ELECTRONS
PROTONS
COROTATION INTERVAL
1.21 MeV
1.00 MeV
A
A'
α_o = 90°
30°
90°
30°
30°
90°
SEC
10^6
10^5
10^4
10^3
0.1
1.0
10
100 MeV
TIME INTERVAL BETWEEN ENCOUNTERS WITH SATELLITE
KINETIC ENERGY - E_e, E_p

Figure 10